Mechanical behavior of circular and square concrete filled steel tube stub columns under local compression

Fa-xing Ding [1], Jing Liu [1*], Xue-mei LIU [2], Zhi-wu Yu [1,3], Da-wen Li [1]

[1] *School of Civil Engineering, Central South University, Changsha, Hunan Province, 410075, P. R. China.*

[2] *School of Civil Engineering and Built Environment, Queensland University of Technology, Brisbane, QLD 4001, Australia*

[3] *National Engineering Laboratory for High Speed Railway Construction, Changsha, 410075, P. R. CHINA*

Abstract：This paper presents both experimental and numerical study on the behaviour of both circular and square concrete-filled steel tube (CFT) stub columns under local compression. Twelve circular and eight square CFT stub columns were tested to study the bearing capacity and a few key parameters. A 3D finite element model was established for simulation and parametric study to investigate the structural behaviour of the stub columns under local compression. The numerical results agreed well with the experimental results. In addition, precise and concise formulas were proposed to calculate the load bearing capacity of CFT stub columns under local compression.

Key words: Concrete filled steel tube; local compression; finite element; ultimate bearing capacity

Symbols	
A_c	Cross-sectional area of concrete
A_s	Cross-sectional area of steel tube
A_{sc}	Cross-sectional area of specimen
A_{cb}	Area of local compress concrete
B	Outside width of the square section
b	Width of loading plate plate
D	Outside diameter of circular steel tube

* Corresponding author, Email address: liujing001@csu.edu.cn

d	Diameter of loading plate plate
DI	Ductility index
E_c	Concrete modulus of elasticity
E_s	Steel modulus of elasticity
E_{st}	Strengthening modulus of steel
f_{cu}	Concrete compressive cube strength
f_c	Uniaxial compressive strength of concrete
f_y	Yield strength of steel
L	Length of the specimens
SI	Strength index
t	Wall thickness of steel tube
K	Confinement coefficient
K_b	Influence coefficient of the CFT stub columns local compression bearing capacity
N	Axial load
N_b	Ultimate load-bearing capacity of locally loaded circular CFT stub columns
$N_{b,e}$	Ultimate load-bearing capacity of locally loaded circular CFT stub columns from experimental results
$N_{b,FE}$	Ultimate load-bearing capacity of locally loaded circular CFT stub columns from FE results
$N_{b,f}$	Ultimate load-bearing capacity of locally loaded square CFT stub columns from formulation
N_u	Axial ultimate bearing capacity
Φ	Confinement index
$\Delta_{85\%}$	Axial deformation when the load falls to 85% of the ultimate bearing capacity.
Δ_b	Axial deformation at the ultimate strength of CFT stub columns subjected to local compression

v_s	Poisson's ratio of steel
v_c	Poisson's ratio of concrete
ε_L	Axial strain of steel
$\varepsilon_{\theta,s}$	Circumferential strain of steel
ε_i	Equivalent strain of steel
ε_y	Yield strain of steel
ε_{st}	Hardening strain of steel
ε_u	Ultimate strain of steel
ρ	Area ratio of steel tube to concrete
β	local compression area ratio

1 Introduction

Concrete filled steel tubular (CFT) columns have been increasingly used in bridges and high-rise buildings. They have much more advantages compared with the ordinary steel or concrete system including high strength and stiffness, high ductility, and large energy absorption capacity [1]. With the benefits of CFT, the use of CFT columns is becoming more commonplace and the performance of concrete filled steel tubes has caught more and more research attentions [1-9]. In most cases, such as the pier of bridges and arch structures, CFT columns are subjected to axially compression loads. Experimental and theoretical researches have been carried out to investigate the behavior of CFT stub columns under local compression and the influencing factors on the load bearing capacity. Forty three circular CFT stub columns under local compression were experimentally studied by Cai et al. [1]. Effects of local compression area ratio, diameter-thickness ratio, relative height of the model and spiral stirrup on the performance and the load bearing capacity were studied. Formula for the ultimate load bearing capacity of CFT stub columns was also proposed. Han et al. [2-3] also conducted experiments to investigate the effects of a few parameters, such as

the section type and local compression area ratio, on the structural behavior of CFT stub columns and proposed a series of formulas for the local compression bearing capacity of CFT stub columns.

The previous study from reference [1-3] indicated that the CFT columns generally perform well, however, little success has been achieved so far in developing a concise formula of the load bearing capacity for CFT stub columns. Moreover, the behavior of CFT columns under local compression condition has not been well addressed in the current design code and hence further research is necessary to further improve the design code specifications. In addition, the effect of loading plate shape on the performance of CFT stub columns may also need to be looked after.

The aim of this study, therefore, is to develop a more concise and precise method to compute the load bearing capacity of CFT stub columns subjected to local axially compression. More specifically, four objectives are included in the study. (1) To analyze the structural behavior of both circular and square CFT stub columns subjected to local compression with 12 circular CFT specimens and 8 square CFT specimens without endplate tested; (2) To develop finite element (FE) model using ABAQUS program to simulate the behavior of the CFT stub columns; (3) To analyze the effects of local compression area ratio, steel ratio, strength of steel and concrete on the behavior of locally loaded CFT specimens; (4) To establish a simplified approach to estimate the load bearing capacity of CFT stub columns subjected to local compression, and to verify formula with both experimental and numerical results.

2 Experimental study

2.1 Test materials and specimens

Twenty CFT specimens were included in this study, including 12 circular and 8 square specimens. The nominal dimension of the circular specimen was 300(D) mm×4(t) mm×900(L) mm, where D is the diameter of the circular section, t is the wall thickness of the steel tube, and L is the length of the specimen. The

nominal dimension of the square specimen was 300(B) mm×4(t) mm×900(L) mm, where B is the width of the square section. d is the diameter of loading plate, b is the width of loading plate. More detailed geometric properties and characteristics of the specimens are presented in Table 1.

In this paper, local compression area ratio is defined as $\beta = A_{cb}/A_{sc}$, where A_{sc} is the cross sectional area of specimen, and A_{cb} is the area subjected to local compressive load. f_y means the yield strength of steel and f_{cu} represents the concrete compressive strength. The main factors considered in the study included concrete strength and local compression area ratio. The steel tubes were molded by bending Q235 steel plates. Butt welds were used according to the standard GB 50017-2003[10] and the ends of the steel grooves (as the sites of welding) were kept smooth after welding.

For the convenience of observation and record of deformation and failure model of the specimen, red paint was sprayed on the external surface of the steel tube and 50mm×50mm white grids were plotted on the surface. A cover plate was initially welded to cover the bottom end of the steel tube before concrete pouring. Concrete was then pumped into the tube from the top and was vibrated to be well compacted and the concrete surface was leveled before finishing. Meanwhile standard concrete cubes with a dimension of 150mm×150mm×150mm and prisms with a dimension of 100mm×100mm×300mm were prepared and cured at the same condition as those of CFT specimens. Grade C30 and C50 commercial concretes were used in this study and the mix design is given in Table 2.

Before testing the columns, material testing was conducted to obtain the respective mechanical properties. The cubic compressive strength f_{cu} of concrete were obtained from the testing of the concrete cubes and the elastic modulus E_c and Poisson's ratio v_c were obtained by testing the concrete prisms according to GB/T 50081-2002 [11]. Tensile coupon tests on 4 mm-thick steel plates were conducted according to GB/T 228-2002 [12]. The obtained material properties are presented in Table 3.

2.2 Experimental method

Depending on the load bearing capacities of each column, local compressive test of the column was conducted either by a 500 ton or a 2000 ton triaxial compressive testing machine in Civil Engineering Safety Science Laboratory at Central South University. The specimens were seated directly on the rigid steel bed of the machine. Figure 1 illustrates the test set-up of specimens and instrumentations. A 40 mm-thick load bearing plate was used for loading. To measure the deformation, five strain gauges (S1-S5) were installed at different vertical position for each specimen. Two linear voltage displacement transducers (LVDTs) (L1-L2) were adopted to measure the axial deformation, as shown in Figure 2. Load-strain/deformation curves were acquired by data acquisition systems for strain gauges and transducers.

The load was applied on the top of the specimen. A load control mode was used and the load was increased at the step of 1/10 of the ultimate load in the elastic stage and at the step of 1/20 of the ultimate load in the elastic-plastic stage, each loading step took 3~5 minutes. The specimens were continuously loaded until failure. The development of cracking, the mode of failure, the deformation, and the load beard by the specimens were all monitored and recorded.

2.3 Experimental results and discussion

The measured axial load versus deformation curves of the CFT specimens are presented in Figure 3. At the beginning of loading, all specimens were in elastic status as indicated by the linear responses of the load versus displacement (N-Δ) curves. When the imposed load reached 60%~70% of the ultimate load, steel tube started to yield and the N-Δ curves gradually demonstrated elastic-plastic behavior. The measured ultimate bearing capacity ($N_{b,e}$) of the specimens are listed in Table 1. It could be found that, the smaller the local compression area ratio was, the smaller the ultimate bearing capacity and elastic modulus were, and the slower the curve dropped down after the peak load. This can be explained that, with a smaller local

compression ratio (β), the steel tube could have weaker confinement to core concrete. In addition, the larger the concrete strength was, the higher the ultimate bearing capacity could be.

The steel tube was expanding due to the local compression and the extent of expansion decreased from the top to the bottom. With the load increasing continuously, once reaching the ultimate load, the end of concrete was obviously crushed and the steel deformation experienced a rapid increase. Lateral dislocation of the columns and crushing of the core concrete were observed when ultimate load was reached. Figure 4 shows the distribution of both axial strain ε_L and circumferential strain $\varepsilon_{\theta,s}$ along the height of the specimens at different loading levels (n) (n=$N/N_{b,e}$, where $N_{b,e}$ is the ultimate load bearing capacity of CFT columns subjected to local compression,). It can be seen from Figure 4, the strain increases slowly at the initial loading stage and it starts to increase rapidly when the load approaches about 70% of the ultimate load. The axial stiffness of CFT columns decreased considerably and both vertical and circumferential load strain curves of the steel showed significant nonlinear responses with the load continuously increased to above 70% of the ultimate load capacity. The circumferential strains at the upper parts of the specimens were the largest, and this was consistent with the observed distortion phenomenon from the experiments. Circular CFT columns had larger strain than the square ones, and it can be explained by the more effective confinement of the steel tube provided to the core concrete by the circular steel tube compared with that provided by the square steel tube.

Figure 5 shows comparison of the different failure modes with varieties of β. In addition to CLST1-A/B and CLST3-A/B with a local compression area ratio of 0.11, the load bearing capacities of the other specimens dropped down significantly after the destruction of the specimens. However, the declining tendency was slower for the circular CFT columns than for square ones as show in Figure 3. It was found that β has significant influence on the failure modes of these specimens. The CFT stub columns experienced outward buckling under the local compression. The bigger the β was, the more significant the confinement

effects of the steel tube on the core concrete was and the larger the outward buckling area and extent of the steel tubes would be.

In order to compare the confinement effect of the circular and square CFT columns under local compression, strength index *SI* on axially local compression is defined by:

$$SI = \frac{N_{\mathrm{b,e}}}{N_u} \tag{1}$$

where N_{u} is the ultimate load bearing capacity of CFT columns.

Figure 6 illustrates the relationship between the strength index (*SI*) and the local compression area ratio (β). The average *SI* was 0.470, 0.838 and 1 in corresponding to the β value at 0.11, 0.44 and 1.00 respectively for circular CFT columns. And the average *SI* was 0.237, 0.556 and 1 in corresponding to the β value at 0.11, 0.44 and 1.00 respectively for square CFT columns. It can be found that *SI* increased with the increase of β. The strength index of the circular CFT columns were larger than that of square ones. This could be attributed to the larger confinement effects from the circular CFT columns than those from the square columns. Besides, *SI* of C50 circular CFT specimens was lower than that of C30 circular columns. However, for the square CFT columns, concrete grade did not influence the *SI* significantly.

For simplification, ductility index for CFT columns subjected to axially local compression is defined by:

$$DI = \frac{\Delta_{85\%}}{\Delta_{\mathrm{b}}} \tag{2}$$

where Δ_{b} is the axial deformation at the ultimate bearing capacity of CFT columns subjected to local compression, $\Delta_{85\%}$ is the axial deformation when the load falls to 85% of the ultimate load bearing capacity.

The relationship between the ductility index (*DI*) and the local compression area ratio (β) is presented in Figure 7. It was found that *DI* was decreased with the increase of β value. In addition, the ductility of the circular CFT columns was much higher than that of the square ones. This may also due to the better confinement to core concrete provided by the circular steel tube than the square one for the composite specimens under local compression loading. The load-displacement curve of the circular CFT specimens

didn't descend when β was 0.11 (Figure 3.), and hence the *DI* value in this case was infinite.

3 FE analysis

3.1 Finite element modeling

Finite element models were established by ABAQUS program [14]. Four-node reduced integral format shell elements (S4R) were employed to model the steel tubes. Eight-node brick elements (C3D8R) were applied to model the concrete, the end plate and the loading plate. . The structured meshing technique was adopted. Mesh convergence studies were first performed to ensure that the finite-element mesh was sufficiently fine to give accurate results and the selected meshed models used for modelling are shown in Figure 8. The type of contact between the steel tube and concrete was defined as surface to surface and coulomb friction model between concrete and steel was adopted for simulation. In the tangential direction, a friction coefficient of 0.5 was used for analysis. The sliding formulation was finite sliding, and a hard contact was defined in the normal direction.

The constraint type between concrete and end plate, concrete and loading plate were tie, because tie constraint can combine two separate surfaces together so that no relative motion occurs between them. The constraint type of shell to solid coupling was applied to model the constraint between steel tube and end plate. In the FE models, one end plate was fixed, the other end of the CFT stub columns were subjected to local compression by a displacement control method. To obtain the complete load-displacement curves with the descending portions, an incremental iteration method was applied. The displacement loading mode was selected to solve the nonlinear equations.

The material constitutive models of concrete used for this study were suggested by Ding et al. [13]. In addition, Plastic-damaged model was adopted for the concrete.

$$y = \begin{cases} \dfrac{kx + (m-1)x^2}{1 + (k-2)x + mx^2} & x \le 1 \\ \dfrac{x}{\alpha_1 (x-1)^2 + x} & x > 1 \end{cases} \tag{3}$$

where k is a ratio of the initial tangent modulus to the secant modulus at peak stress and equals to $9.1 f_{cu}^{-4/9}$. m is a parameter that controls the decrease in the elastic modulus along the ascending portion of the axial stress-strain relationship and equals to $1.6(k-1)^2$. For a CFT stub column, parameter α_1 can be taken as 0.15.

The Poisson ratio v_c of concrete was taken as 0.2. Equation (3) is able to describe the stress-strain relationship of concrete with strengths ranging from 20MPa to 140MPa which has been validated by experimental results [13].

An elasto-plastic model, with consideration of Von Mises yield criteria, Prandtl-Reuss flow rule, and isotropic strain hardening, was used to describe the constitutive behavior of steel. The expression for the stress-strain relationship of steel is as below [13].

$$\sigma_i = \begin{cases} E_s \varepsilon_i & \varepsilon_i \le \varepsilon_y \\ f_s & \varepsilon_y < \varepsilon_i \le \varepsilon_{st} \\ f_s + \zeta E_s (\varepsilon_i - \varepsilon_{st}) & \varepsilon_{st} < \varepsilon_i \le \varepsilon_u \\ f_u & \varepsilon_i > \varepsilon_u \end{cases} \tag{4}$$

where σ_i is the equivalent stress of steel; f_s is the yield strength; f_u is the ultimate strength and $f_u = 1.5 f_s$; E_s is the elastic modulus, $E_s = 2.06 \times 10^5$MPa; E_{st} is the strengthening modulus, which is described by $E_{st} = \zeta E_s$; ε_L is the equivalent strain; ε_y is the yield strain; ε_{st} is the strengthening strain; and ε_u is the ultimate strain, which is described by $\varepsilon_u = \varepsilon_{st} + 0.5 f_s / (\zeta E_s)$, where $\varepsilon_{st} = 12\varepsilon_y$, $\varepsilon_u = 120\varepsilon_y$ and $\zeta = 1/216$.

3.2 Failure mode and load-deformation curve

Figure 9 presents the stress distribution of different CFT columns under local compression and the stress contour also indicates the failure modes of these CFT specimens through FE analysis. Comparing Figure 9

and Figure 5, it was found that the numerical results were in good agreement with the experimental results. The comparison of the typical *N-Δ* curve between FE analysis and experimental results on CFT stub columns under local compression is presented in Figure 10. The comparison indicated that the FE model provided reliable prediction on the load-displacement behavior of the CFT stub columns and also demonstrated its capability to evaluate the behavior of local loaded CFT columns with a reasonable accuracy.

3.3 Effect of the loading plate shape

The effect of loading plate shape on the mechanical behavior of CFT stub columns under local compression was investigated. Three types of plate section, circular, square, rectangle shape, were selected for investigation, the aspect ratio of rectangle loading plate was 2:1. The influence of loading plate shape on the *N-Δ* curve is presented in Figure 11.

When β=0.11, the load bearing capacity of the circular CFT columns is 0.94% higher when using a circular loading plate than that using a square loading plate and the value was 7.31% higher when using a rectangle loading plate than that using a square loading plate. Moreover, the load bearing capacity of the square CFT columns is 0.13% higher when using a circular loading plate than that using a square loading plate and the value was 2.95% higher when using a rectangle loading plate than that using a square loading plate.

When β=0.44, the load bearing capacity of the circular CFT columns is 8.05% higher when using a circle loading plate than that using a rectangle loading plate and the value was 13.43% higher when using a square loading plate than that using a rectangle loading plate. Also, the load bearing capacity of the circle CFT columns is 6.27% higher when using a rectangle loading plate than that using a circular loading plate and the value was 9.97% higher when using a square loading plate than that using a rectangle loading plate.

It can be concluded that when the β was small (β=0.11), the shape of the loading plate has minimal

effect on the load bearing capacity of the CFT columns. When the β was big(β=0.44), compared to the shape of circle and square loading plate, using a rectangle loading plate own the smallest load bearing capacity of CFT columns, and the difference between the circle and square loading plate was minor.

3.4 Parametric study

The validated FE model was further used for parametric study to understand the influence of local compression area ratio (β), steel ratio (ρ, area ratio of steel tube to concrete), steel and concrete strength (f_y and f_{cu}) on the structural performance of CFT columns. The parameters used for the study were detailed as below. (1) The wall thickness of the steel tube were set as 7 mm, 12 mm, and 17 mm; (2) The external diameter of the cross section of the circular CFT column and the width of the cross section of the square CFT column were 500 mm; (3) The depth of the cross section of the square column was set as 1500 mm; (4) The local compression area ratio were set as 0.09, 0.36, 0.64 and 1.00. The diameter or width of loading plate were 150 mm, 300 mm, 400 mm and 500 mm respectively. (5) The selected compressive strength of concrete was 30, 40, 50, and 60 MPa, (6) Different yield strengths of steel 235, 335, and 420 MPa were used. The following steel and concrete were paired for the CFT columns: Q235 steel paired with C30 and C40 concrete, Q335 steel paired with C40 and C50 concrete, Q420 steel paired with C50 and C60 concrete. (7) 72 circular and 72 square CFT stub columns were investigated in parametric study. Figure 12 presents the influence of various parameters on the N-Δ curve. Each parameter was discussed below.

Figure 12(a) presents the typical N-Δ curve of CFT stub columns with both square and circular section with different β values. It was found that, β had significant impact on the load bearing capacity of CFT stub columns, and the load bearing capacity increased with the increase of local compression area ratio. Figure 12(b) illustrates the effect of ρ on N-Δ curve of the CFT stub columns. It can be seen that, the larger the ρ was, the higher the load bearing capacity and elastic stiffness were. There was no descending portion when ρ

reached a certain value. Figure 12(c) demonstrates the relationship between f_y and the N-Δ curve of CFT stub columns. It can be found that, the load bearing capacity was increased as the f_y was increased, but the elastic stiffness was not changed. Figure 12(d) shows the influence of f_{cu} on the N-Δ curve of CFT stub columns. It can be seen that, both the load bearing capacity and the elastic stiffness were increased with the increase of f_{cu}.

Previous model has also considered those above-mentioned parameters by using a influence coefficient K_b to calculate of the load bearing capacity of the CFT columns under local compression. According to [5] the axial bearing capacity N_u of the CFT stub column can be determined by:

$$N_u = f_c A_c (1 + K\Phi) \tag{5}$$

where Φ is the confinement index, $\Phi = f_y A_s / (f_c A_c)$. K is the confinement coefficient. K=1.7 for circular CFT columns [5] and K=1.2 for square CFT columns [9]. And the load bearing capacity of CFT stub columns subjected to local compression N_b was recommended to be:

$$N_b = K_b (1 + K\Phi) f_c A_{cb} \tag{6}$$

Where K_b is the influence coefficient and is mainly affected by area ratio, steel ratio, both steel and concrete strengths. Parametric study was also conducted to further understand how K_b is influenced by those parameters and the findings are presented in Figure 13. It indicates that the pressure area ratio is the most vital parameter for the bearing capacity of CFT stub columns. The larger the pressure area ratio was, the larger the influence coefficient was.

4 Formula for load bearing capacity of CFT stub column under local compression

4.1 Formula development

With analysis of experimental results and by using regression method, formula for influence coefficient K_b and load bearing capacity under local compression N_b were developed. For circular CFT columns, K_b is

expressed as:

$$K_b = \beta^{0.05\Phi-0.65} \tag{7a}$$

For square CFT columns, K_b is expressed as:

$$K_b = \beta^{0.05\Phi-0.4} \tag{7b}$$

The load bearing capacity of circular CFT columns under local compression can be written as:

$$N_b = \beta^{0.05\Phi-0.65}(1+1.7\Phi) f_c A_{cb} \tag{8a}$$

The load bearing capacity of square CFT columns under local compression was proposed as:

$$N_b = \beta^{0.05\Phi-0.4}(1+1.2\Phi) f_c A_{cb} \tag{8b}$$

4.2 Formula validation

The load bearing capacity obtained by using Equation (8) ($N_{b,f}$), FE results ($N_{b,FE}$), and experimental results ($N_{b,e}$) as all listed in Table 1. The comparison between the predicted value by Equation (8) and the FE modelling results is summarized in Figure 14 for both circular and square CFT stub columns. Well agreement has been achieved with the maximum discrepancy less than 10%. The comparison between the predicted value by Equation (8) and the experimental results [1-2] is summarized in Figure 15 for both circular and square CFT stub columns. The comparison suggests that Equation (8) provides a good prediction for the load bearing capacity of locally loaded CFT columns. The good agreements indicate that the proposed formulas are reasonable with acceptable accuracy for CFT stub column design and analysis.

Formulas (Equation (9) in Table 4) used for the similar purpose to predict the load bearing capacity of CFT columns under local compression was proposed in [3]. To address the benefits of using Equation (8) over other equation, comparison study was conducted. In addition, the results were also compared with the FE modelling results. Equations (8) and (9) and FE modelling method were applied to predict the load bearing capacity of those CFT columns as tested in this study and also from references [1-2]. The

experimental results were compared with the predicted results using different methods: FE model, Equations (8) and (9). And the ratios of the experimental result over the predicted value by using each individual method are presented in Table 5. It was found, for each group of CFT columns from different studies, FE modelling gives the most accurate prediction with minimum discrepancies as indicated by the coefficient of variation.

For the circular CFT columns, When considering the total 47 groups circular CFT stub columns tested from current study and also the references [1-2], the average $N_{b,e}/N_b$ ratio was 1.038 with a coefficient of variation at 0.165 for Equation (8), and the average $N_{b,e}/N_b$ ratio was 1.059 with a coefficient of variation of 0.255 for Equation (9). Therefore, in general, in predicting of the load bearing capacity of circular CFT stub columns, Equation (8) provided higher accuracy results and little coefficients of variation than Equation (9).

For the square CFT columns, when predicting the load bearing capacity of columns from reference [2] and this paper, the average $N_{b,e}/N_b$ ratio was 0.967 with a coefficient of variation at 0.160 for Equation (8), and the average $N_{b,e}/N_b$ ratio was 0.936 with a coefficient of variation of 0.142 for Equation (9). In general, when considering the prediction results for square CFT stub columns, Equation (8) provided more accurate results than Equation (9), and the coefficient of variation using Equation (8) is slightly higher than using Equation (9).

5 Conclusions

This paper presents both experimental and numerical study on the behavior of both circular and square concrete filled steel tube (CFT) stub columns subjected to local axial compressive loading. Parametric studies were also conducted in order to understand the influence of different parameters on the behavior of the CFT stub columns. Based on the results, the following conclusions can be drawn:

(1) The experimental results indicate that as the increase of concrete strength could increase the load bearing capacities of both circular and square CFT stub columns. The CFT stub columns in circular

section had a higher bearing capacity and a better ductility than those in square section. The experimental results indicated that the local compression area ratio β has significant influence on the failure modes and load bearing capacity of the CFT stub columns. The CFT stub columns experienced outward buckling under the local compression. The larger the β was, the more significant the confinement effects of the steel tube on the core concrete was and the larger the outward buckling area and extent of the steel tubes would be.

(2) A 3D finite element model was established to simulate the structural behavior of both circular and square CFT stub columns subjected to compression loading based on a reasonable material constitutive model by utilizing ABAQUS program. The numerical results were in good agreement with the experimental results.

(3) Based on the parametric study, the pressure area ratio was found to be the most vital parameter for the load bearing capacity of CFT stub columns under local compression. Both steel and concrete strength had significant influence on the load bearing capacity of the CFT stub columns. The load bearing capacity of the CFT stub column was increased as the steel strength was increased, but the elastic stiffness was not changed, both the ultimate strength and the elastic stiffness were increased with the increase of concrete strength.

(4) With analysis of experimental results and by using regression method, formulas for predicting the load bearing capacity of CFT stub columns with both circular and square sections under local compression were developed. The results obtained from the proposed formulas were reasonably consistent with the experimental results. And with reasonable accuracies, the proposed formulas could be more precise, concise and easier for use when compared with the previous method.

(5) It was found the influence of shape of the loading plate on the ultimate strength of the CFT stub columns under local compression was minimal when the β was small, however, there is a

difference between circle and square with rectangle loading plate when the β was big.

Acknowledgment

This research work was financially supported by the Program for Changjiang Scholars and Innovative Research Team in University (PCSIRT), Grant No. IRT1296, the Program for New Century Excellent Talents in University, Grant No. NCET-11-0508, and the National Key Technology R&D Program, Grant No.2011BAJ09B02.

Refrences

[1] Cai SH. Modern steel tube confined concrete structures[M]. Beijing: China communications press, 2003.(in Chinese)

[2] Han LH, Liu W, Yang YF. Behavior of thin walled steel tube confined concrete stub columns subjected to axially local compression [J]. Thin-Walled Structures. 2008, 46(2): 155-164.

[3] Yang YF, Han LH. Experiments on rectangular concrete-filled steel tubes loaded axially on a partially stressed cross-sectional area [J]. Journal of Constructional Steel Research。2009, 65 (8):1617-1630.

[4] Yu ZW, Ding FX, Cai CS. Experimental behavior of circular concrete-filled steel tube stub columns[J]. Journal of Constructional Steel Research, 2007, 63(2): 165-174.

[5] Ding FX, Yu ZW, Bai Y. Elasto plastic analysis of circular concrete-filled steel tube stub columns[J]. Journal of Constructional Steel Research. 2011, 67(10): 1567-1577.

[6] Chang X, Wei YY, Yun YC. Analysis of steel-reinforced concrete-filled steel tubular (SRCFST) columns under cyclic loading, Construction and Building Materials.2012, 28: 88-95.

[7] Lu ZH, Zhao YG. Suggested empirical models for the axial capacity of circular CFT stub columns[J]. Journal of Constructional Steel Research, 2010, 66(6): 850-862.

[8] Chang X, Ru Zl, Zhou W, Zhang Yongbin. Study on concrete-filled stainless steel carbon steel tubular (CFSCT) stub columns under compression. Thin-Walled Structures, 2013, 63: 125-133.

[9] Ding FX, Fang CJ, Bai Y, et al. Mechanical performance of stirrup-confined concrete-filled steel tubular stub columns under axial loading[J]. Journal of Constructional Steel Research, 2014, 98(7): 146-157.

[10] GB 50017-2003. Design of steel structures [S]. Beijing: China Planning Press, 2003.(in Chinese)

[11] GB/T 50081-2002. Standard for method of mechanical properties on ordinary concrete[S] Beijing: China Building Industry Press, 2002.(in Chinese)

[12] GB/T 228-2002. Metallic materials-tensile testing at ambient temperatures [S] Beijing: Standards Press of China,2002.(in Chinese)

[13] Ding FX, Ying XY, Zhou LC, et al. Unified calculation method and its application in determining the uniaxial mechanical properties of concrete [J]. Front. Archit. Civ. Eng. China. 2011, 5(3): 381-393.

[14] Hibbitt, Karlson, Sorenson. Abaqus Version 6.4: Theory manual, users' manual, verification manual and example problems manual [M]. Hibbitt, Karlson, Sorenson Inc., 2003.

Table 1 Geometric properties and characteristics of steel tubes specimens

No.	Section type	Specimen label	$B(D)\times t\times L/mm$	$b(d)$/ mm	f_y/ MPa	f_{cu}/ MPa	β	$N_{b,e}$/ kN	$N_{b,FE}$/ kN	$N_{b,f}$/ kN
1	Square	CLST1-A	300×3.72×900	100	311	35.5	0.11	1880	1630	1908
2		CLST1-B	300×3.76×900	100	311	35.5	0.11	1900	1638	1922
3		CLST2-A	300×3.70×900	200	311	35.5	0.44	3310	2758	2856
4		CLST2-B	300×3.68×900	200	311	35.5	0.44	3200	2750	2848
5		C1-A	300×3.70×900	300	311	35.5	1.00	3780	3757	3625
6		C1-B	300×3.71×900	300	311	35.5	1.00	3540	3763	3630
7		CLST3-A	300×3.69×900	100	311	54.4	0.11	2090	2189	2255
8		CLST3-B	300×3.76×900	100	311	54.4	0.11	2090	2205	2281
9		CLST4-A	300×3.70×900	200	311	54.4	0.44	3810	3656	3620
10		CLST4-B	300×3.77×900	200	311	54.4	0.44	3950	3683	3651
11		C2-A	300×3.74×900	300	311	54.4	1.00	4896	5146	4977
12		C2-B	300×3.87×900	300	311	54.4	1.00	4976	5025	4851
13	Circular	SLST1-A	300×3.68×900	100	311	35.5	0.11	1140	882	994
14		SLST1-B	300×3.68×900	100	311	35.5	0.11	950	882	994
15		SLST2	300×3.70×900	200	311	35.5	0.44	2420	2324	2400
16		S1	300×3.75×900	300	311	35.5	1.00	4370	4060	3985
17		SLST3-A	300×3.72×900	100	311	54.4	0.11	1340	1312	1467
18		SLST3-B	300×3.72×900	100	311	54.4	0.11	1280	1312	1467
19		SLST4	300×3.72×900	200	311	54.4	0.44	3100	3265	3359
20		S2	300×3.70×900	300	311	54.4	1.00	5570	5555	5443

Table 2 Mix design of concrete

Concrete strength(MPa)	Cement(kg/m^3)	Sand(kg/m^3)	Water(kg/m^3)	Aggregate(kg/m^3)
C30	429	536	185	1250
C50	478	610	172	1186

Table 3 Properties of steel and concrete

Material	$f_y(f_c)$/MPa	$f_u(f_{cu})$/MPa	$E_s(E_c)$/MPa	$v_s(v_c)$
Steel plate	311	460	2.07×10^5	0.29
C30	25.7	35.5	3.12×10^4	0.23
C50	42.4	54.4	3.60×10^4	0.23

Table 4 Formulas for bearing capacity of CFT stub columns under local compression

Section	Reference	Formulation	
Circular	[3]	$N_{b,f}= K_b N_u$; $K_b= A\beta_1+B\beta_1^{0.5}+C$; $\beta_1=A_c/A_{cb}$; $N_u=A_c f_c(1.14+1.02\Phi)$; $A=(-0.18\Phi^3+1.95p^2-6.89\Phi+6.94)/100$; $B=(1.36\Phi^3-13.92\Phi^2+45.77\Phi+60.55)/100$; $C=(-\Phi^3+10\Phi^2-33.2\Phi+150)/100$;	(9a)
Square	[3]	$N_{b,f}= K_b N_u$; $K_b= A\beta_1^{-0.5}+B$; $\beta_1=A_c/A_{cb}$; $N_u=A_c f_c(1.18+0.85\Phi)$;	(9b)

A=(-1.38Φ+105)/100;
B=(1.5Φ-5.2)/100;

Table 5 CFT stub columns comparison between calculated and tested ones

Column section	Source of the specimens	Total number of specimens	Characteristic value	$N_{b,e}/N_b$		
				FE	Eq.(8)	Eq.(9)
Circular	this paper	12	Average	1.014	1.049	1.152
			Coefficient of variation	0.042	0.093	0.055
	Reference [1]	27	Average	0.968	1.071	0.996
			Coefficient of variation	0.241	0.187	0.341
	Reference [2]	8	Average	0.962	0.924	1.134
			Coefficient of variation	0.092	0.121	0.082
	All above	47	Average	0.973	1.038	1.059
			Coefficient of variation	0.133	0.165	0.255
Square	this paper	8	Average	1.013	0.986	0.935
			Coefficient of variation	0.074	0.081	0.128
	Reference [2]	28	Average	0.970	0.962	0.936
			Coefficient of variation	0.132	0.178	0.148
	All above	36	Average	0.975	0.967	0.936
			Coefficient of variation	0.115	0.160	0.142

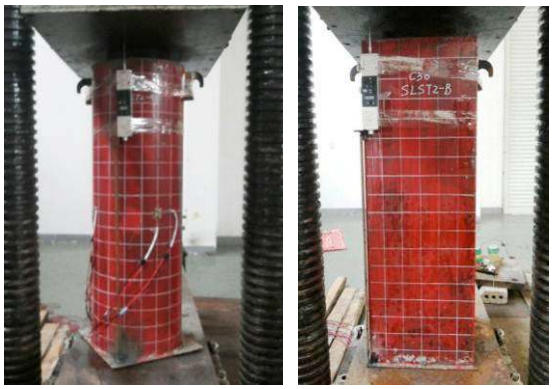

(a)Circular CFT (b) Square CFT

Fig.1. Experimental setup

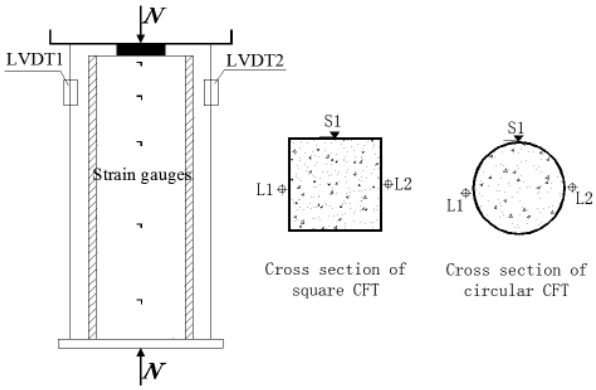

Fig.2. Test specimen and instrumentation.

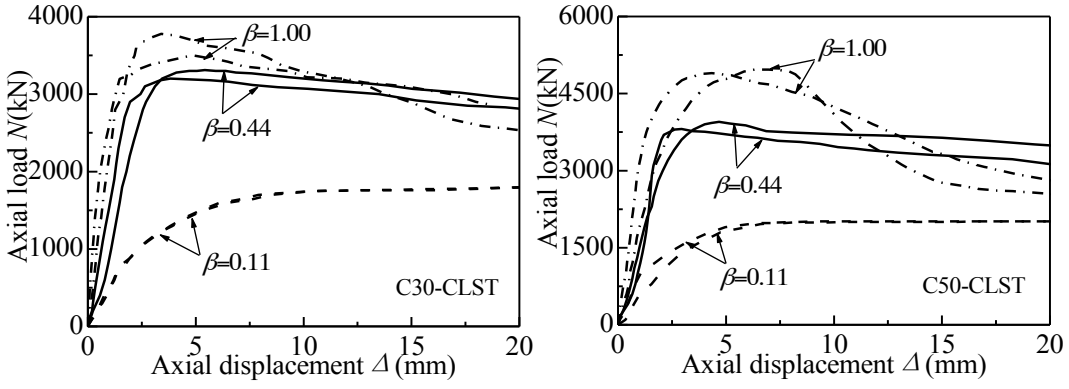

(a)C30-Circular CFT (b) C50-Circular CFT

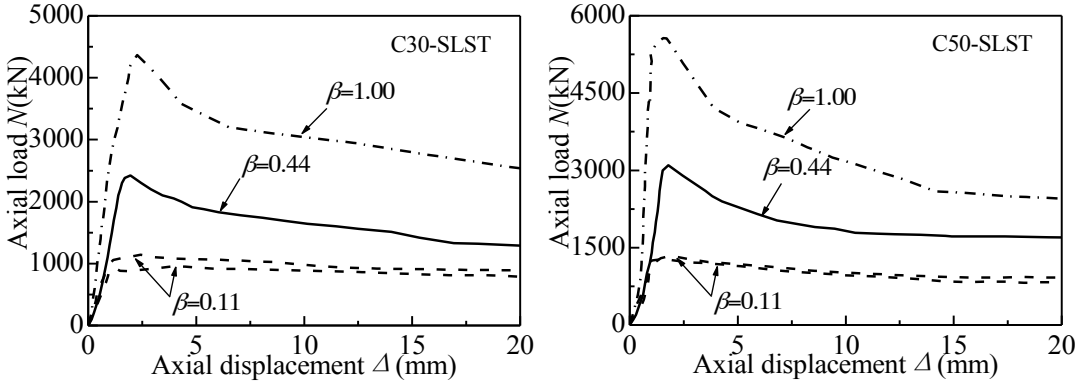

(c) C30-Square CFT (d) C50-Square CFT

Fig.3. Load (N) versus deformation (Δ) relationships of CFT specimens.

Fig.4. Axial strain (ε_L) and circumferential strain ($\varepsilon_{\theta,s}$)of specimens along axial direction.

β=0.11 β=0.44 β=1.00

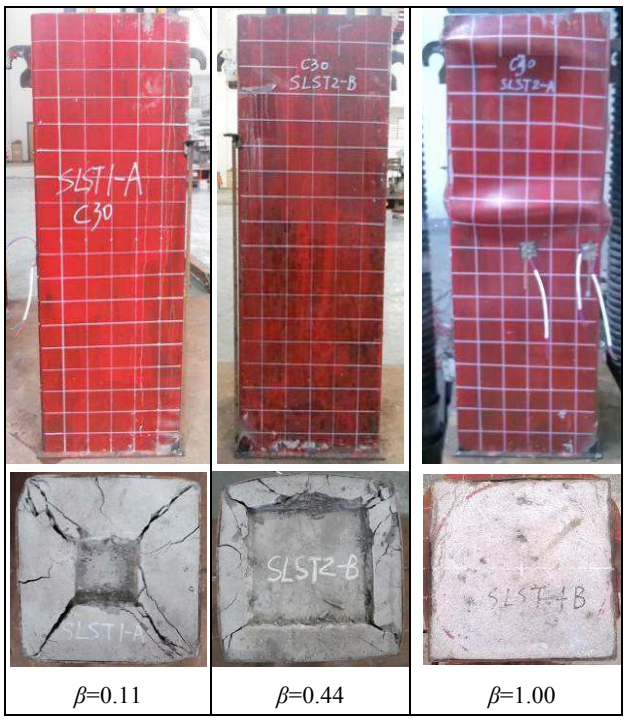

Fig.5. Comparison on the typical failure model of the columns.

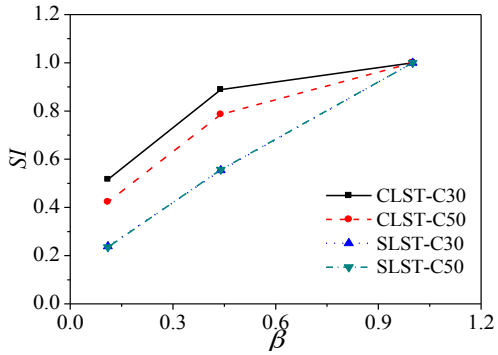

Fig.6. Relationship between *SI* and *β*.

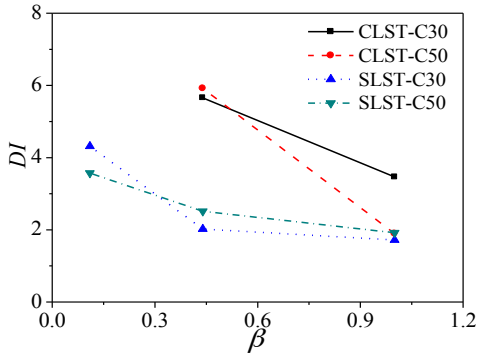

Fig.7. Relationship between *DI* and *β*

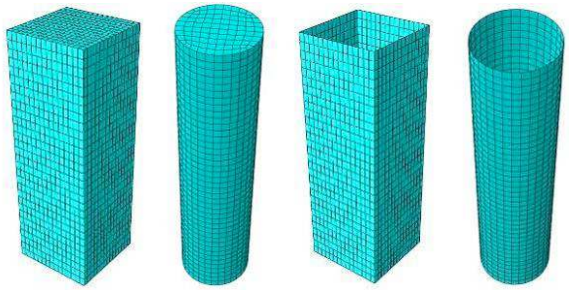

(a) Element of concrete and steel

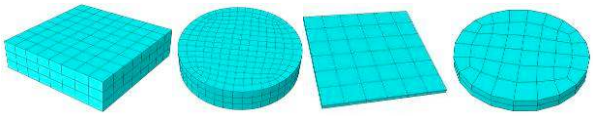

(b) Element of loading plate and base plate

Fig.8. The meshed FE models.

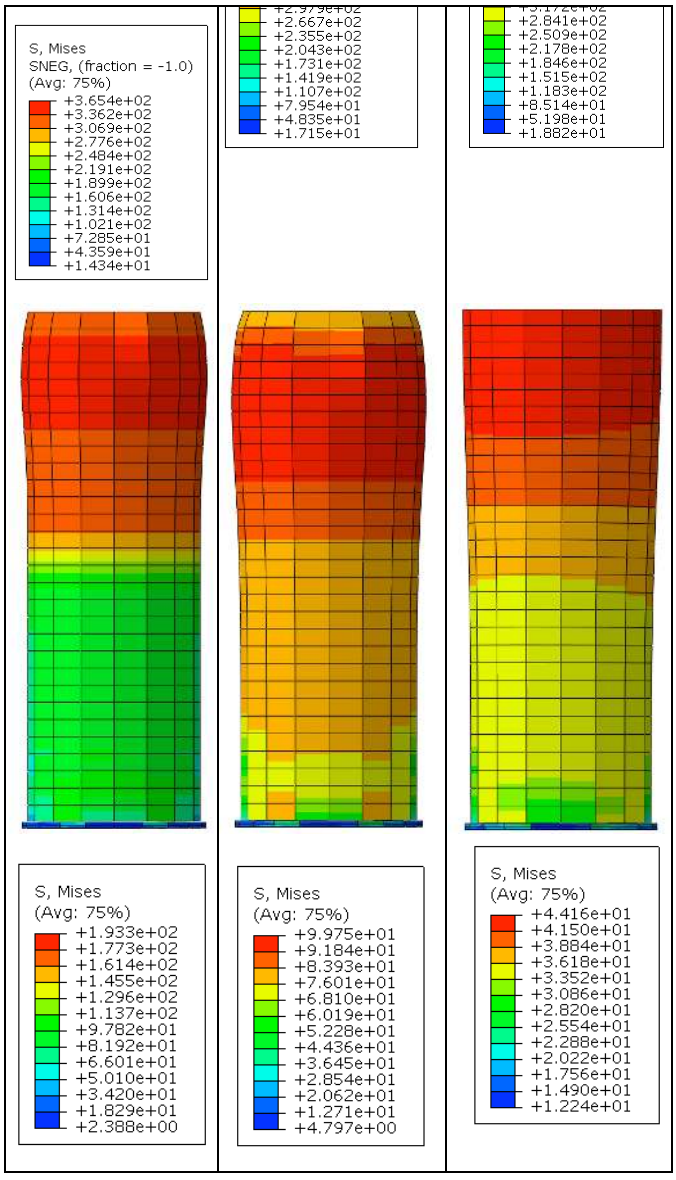

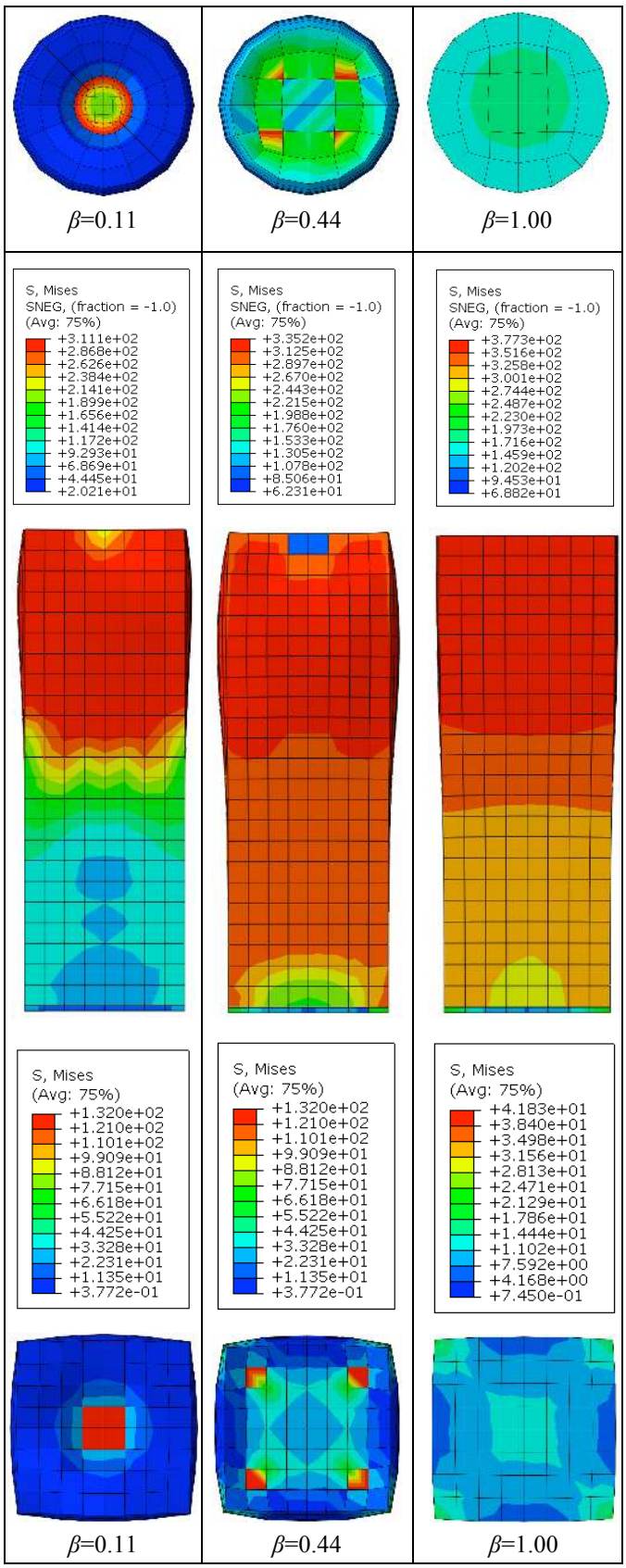

Fig.9Stress contours of different columns under local compression.

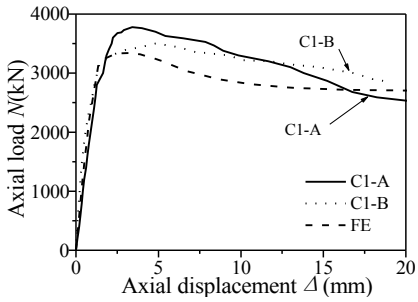

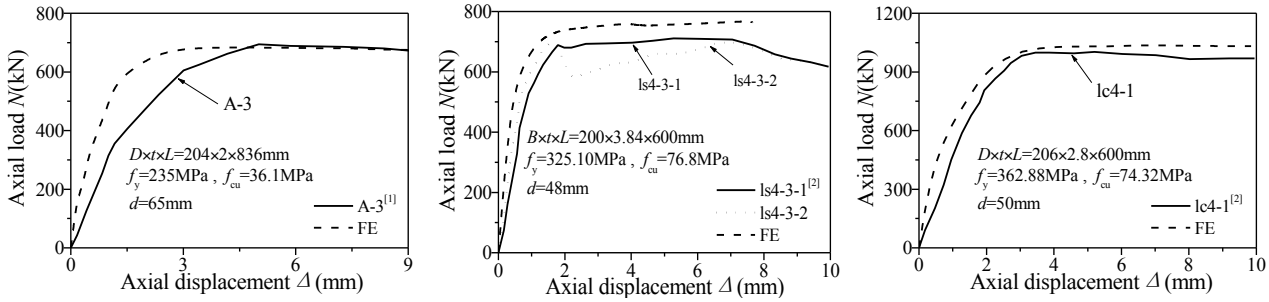

Fig.10. Comparison of *N*-*Δ* curves obtained from FE models and experiments.

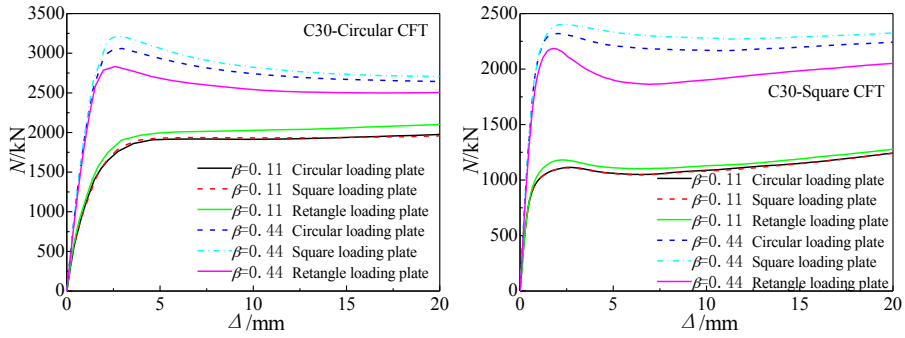

Fig.11. Influence of loading plate shape on the *N*-*Δ* curves.

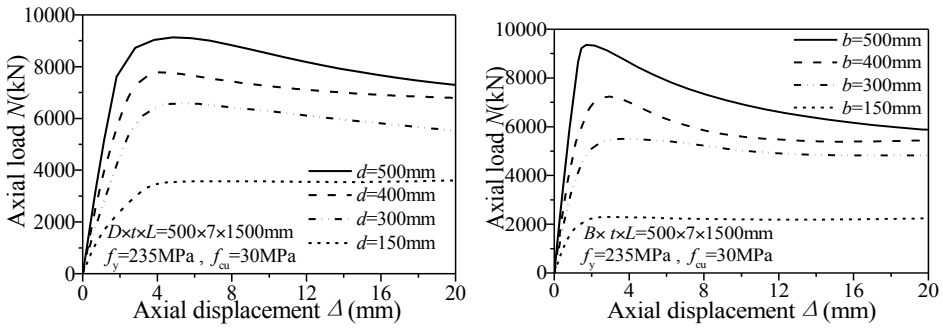

(a) Influence of local compression area ratio

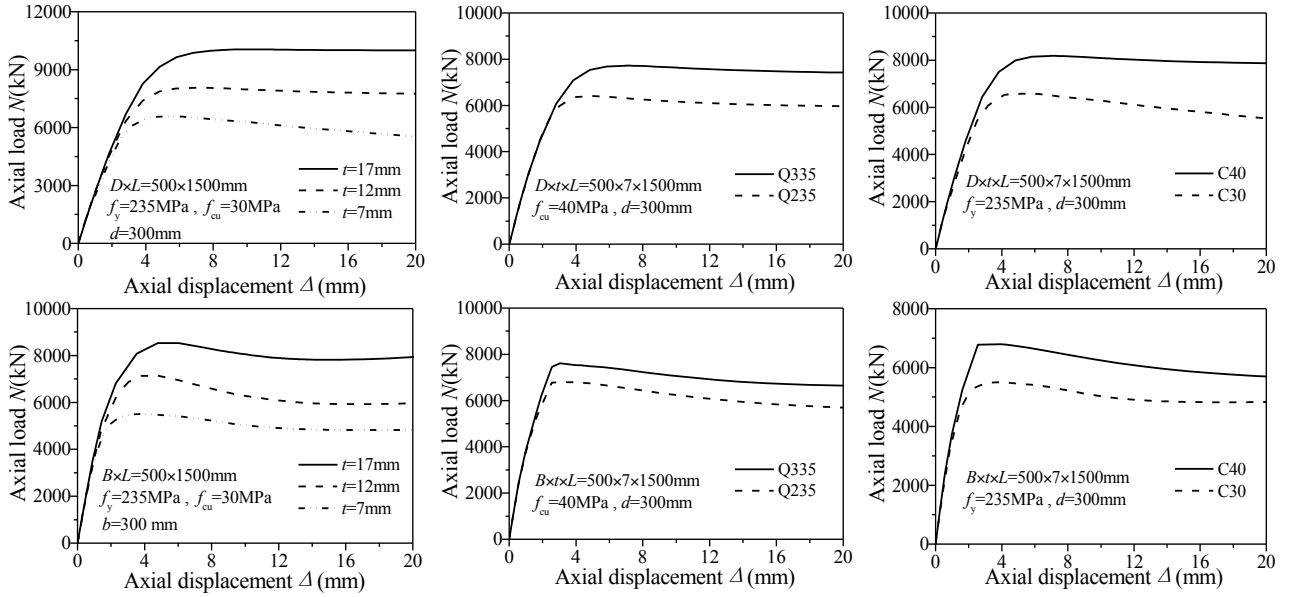

(b) Influence of steel ratio (c) Influence of steel strength (d) Influence of concrete strength

Fig.12. Influence of various parameters on the Load *N-Δ* curve.

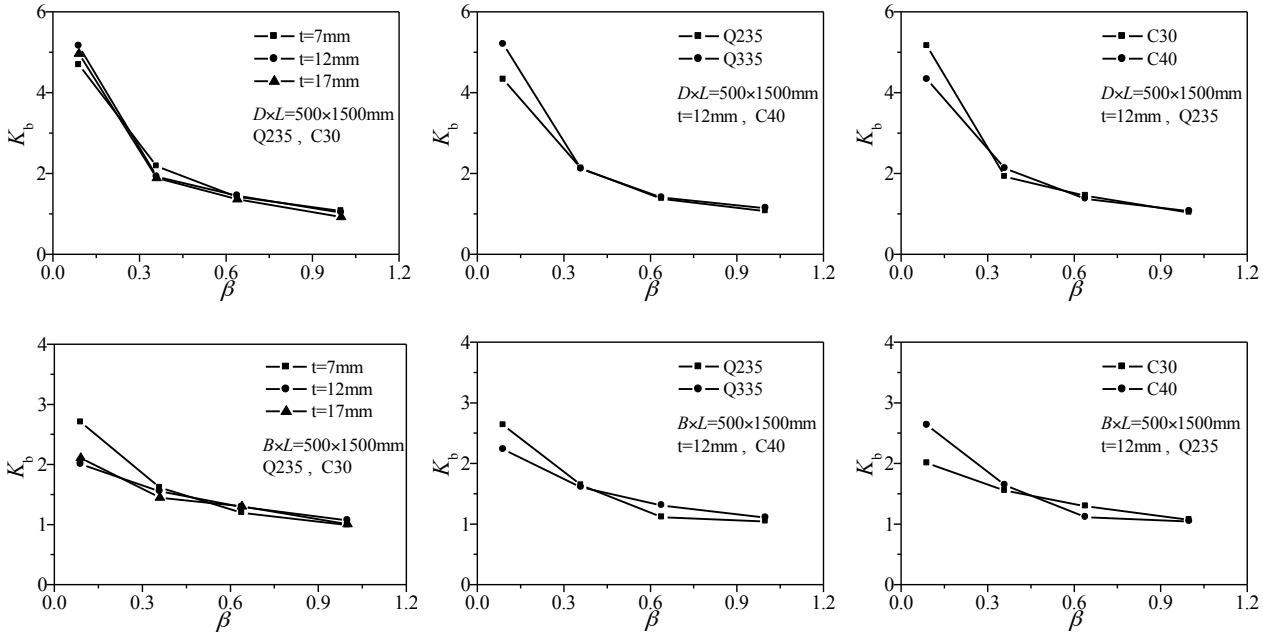

(a) Influence of steel ratio (b)Influence of steel strength (c)Influence of concrete strength

Fig.13. Influence of different parameters on K_b.

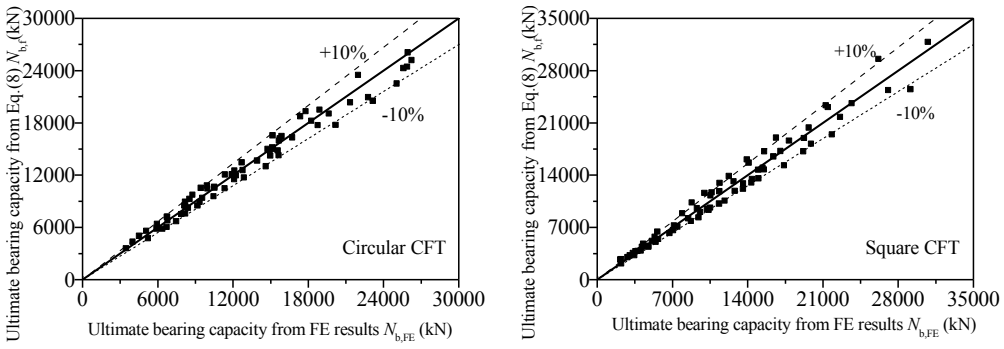

(a) Circular CFT (b) Square CFT

Fig.14. Comparison of the bearing capacity obtained from FE model and Eq.(8).

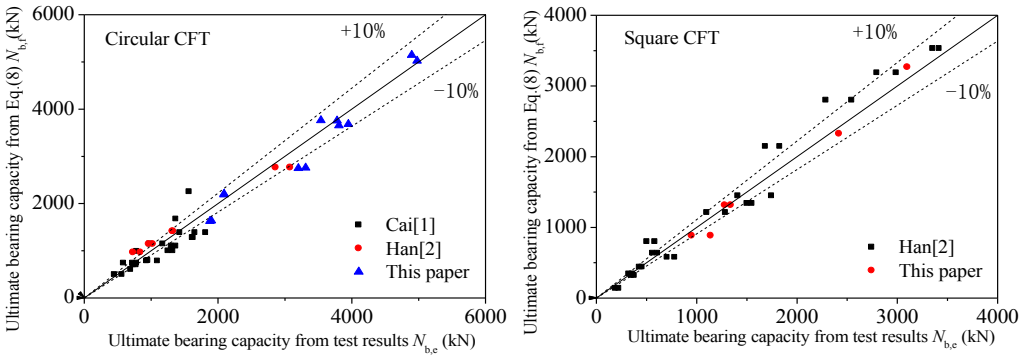

(a)Circular CFT (b) Square CFT

Fig.15. Comparison of the bearing capacity obtained from Eq.(8) and experiments.